A peridynamic model for damage prediction of fiber reinforced composite laminate

Bo Ren, C. T. Wu

Livermore Software Technology Corporation, 7374 Las Positas Road, Livermore, CA 94551-5110, United States

ABSTRACT

This paper presents the keywords for a bond-based peridynamic model in LS-DYNA® to predict the damage of fiber reinforced composite laminates. To represent the anisotropy of a laminate by the peridynamic model, a lamina is simplified as a transversely isotropic media under the plane stress condition. The laminated structure is modeled by stacking the surface mesh layers along the thickness direction according to the laminate sequence. The bond stiffness can be evaluated using the engineering material constants, based on the equivalence between the elastic energy density in the peridynamic theory and the elastic energy density in the classic continuum mechanics theory. Benchmark tests are conducted to verify the proposed model. The numerical results illustrate that the elastic behavior of a laminate can be simulated accurately in comparison to experimental data. In terms of damage analysis, the proposed model can capture the dynamic process of the complex coupling of the inner-layer and delamination damage modes.

Keywords: Peridynamic theory, Discontinuous Galerkin theory, Fiber reinforced composite laminate, Damage process, Arbitrary fiber orientation

1. Introduction

Fiber reinforced composites are extensively adopted in modern structural design, especially in the automotive and aerospace industries. Because of the heterogeneous nature and complex damage patterns observed in laminated composites, the numerical models for damage simulation in these materials are remaining challenge after decades of research efforts in this field [1-2]. This paper provides a peridynamic material model for fiber reinforced composite laminates, which can represent anisotropy with arbitrary fiber orientation without mesh dependency. Following Ghajari et al. [3], the micro-elastic modulus distributive pattern in the principal material coordinate system can be described by a spherical harmonic expansion. Basing on this function, Peridynamic bonds are classified to two types: inner layer bonds and inter layer bonds. Instead of modeling brittle fracture as a quasi-static problem, the 3D explicit dynamics bond-based peridynamic formulas are constructed with the discontinuous Galerkin theory [4].

The reminder of this paper is as follows. In section 2, the keywords for LS-DYNA® peridynamic model are presented. Section 3 presents several benchmark problems. Final remarks are given in Section 4.

2. Keywords for the peridynamics model in LS-DYNA®

The bond-based peridynamic model in LS-DYNA® is implemented in FEM framework with discontinuous Galerkin theory [4]. It is a new element formulation, therefore, a keywords is need to define the peridynamic section:

***SECTION_SOLID_PERI**

This keyword has two parameter cards:
Card 1

Variable	SECID	ELFORM
Type	I	I
Default		

SECID: The section ID
ELFORM: Element formulation. Equals 48. Peridynamic section supports 3-nodes and 4-nodes elements. Comparing with the regular FEM mesh, peridynamic mesh uses discontinuous mesh, i.e., each element has its own node index, the adjacent elements don't share nodes as Fig. 1. This discontinuous mesh can be built from a regular FEM mesh by detach nodes in LS-PrePost®

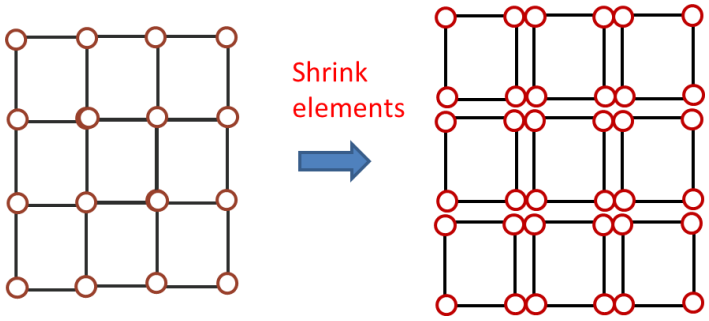

Fig. 1. Discontinous mesh for peridynamic model

Card 2

Variable	DR	PTYPE
Type	F	I
Default	1.01	1

DR: normalized horizon size, 1.0 is recommended
PTYPE EQ.1: bond based formulation
DR is the user defined reference support size which is normalized with the maximum element diagonal length. For those extreme irregular mesh, LSDYNA will adjust DR automatically to make sure the neighbor number of a point is $10 \leq n_g \leq 136$.

***MAT_ELASTIC_PERI_LAMINATE**

This keyword defines a transverse isotropic elastic material for one ply in laminates, which is the material model only available for peridynamic laminate model, and has 2 parameter cards:
Card 1

Variable	**MID**	**RO**	**Ef**	**Em**	**vfm**	**FOPT**	**FCf**	**FCm**
Type	I	F	F	F	F	I	F	F
Default								

MID: User defined material ID
RO: mass density
Ef: E1, Young's modulus-longitudinal direction for one lamina. 1-direction
Em: E2, Young's modulus-transverse direction for one lamina. 2-direction
vfm: v12 Poisson's ration in the ply plane, FOPT: failure criteria type:
1: Energy release rate
2: Failure stretch ratio for tension
FCf: Failure criteria for longitudinal direction, 1-direction
FCm: Failure criteria for transverse direction,2-direction
One lamina layer is considered as a transverse isotropic material. It's a 2D material model.
Basically, the energy release rate, G, is recommended as the failure criteria.
Card 2

Variable	**V1**	**V2**	**V3**
Type	F	F	F
Default			

V1,V2,V3: Locally orthotropic premier material axes (1-,2-,3- axes) determined by the cross product of a vector in the plane of the element (v1,v2,v3) with the element normal.
* SET_PERI_LAMINATE
This keyword assembles the sections assigned *MAT_ELASTIC_PERI_LAMINATE to laminate. This keyword has 2 or more cards:
Card1:

Variable	**SID**
Type	I
Default	

SID: The set id
Card 2:

Variable	**PID1**	**A1**	**T1**	**PID2**	**A2**	**T2**
Type	I	F	F	F	F	I
Default						

PID*: The part id for the first and second lamina.
A*: The fiber angle in this lamina. The 0 degree angle is defined by (v1,v2,v3) in keyword.
T*: the thickness of this lamina.

Card 2 can repeat until all lamina layers are define

*** ELEMENT_SOLID_PERI**

Unlike the regular solid elements, which are 3D elements, the element for laminate in peridynamic model are surface elements: 3-nodes or 4-nodes elements. This keyword has 1 card:

Variable	eid	pid	n1	n2	n3	n4
Type	I	F	F	F	F	I
Default						

eid*: the element id.

pid: part id

n1,n2,n3,n4: the node index for this element. The peridynamic laminate model use 4 nodes element mesh. It's shell element geometrically, but it's not shell element formula.

3. Numerical examples

In this section, two benchmark examples are analyzed using the proposed peridynamic model to demonstrate its application to the fracture analysis of fiber reinforced composite laminates. The numerical time integration of the discrete equation is performed by the regular central difference method. The standard bilinear shape functions of four nodes elements with 2×2 Gaussian points per element is used for all examples. For all numerical examples, the horizon $\delta = 0.8 * l_e$ (l_e: the diagonal length of each element) is utilized, which implies that δ is a distributive value in a computational domain depending on element size. The time step is fixed at $\Delta t = 10^{-7} s$ for all the tests in this study.

3.1 The compact-tension test of a transversely isotropic plate

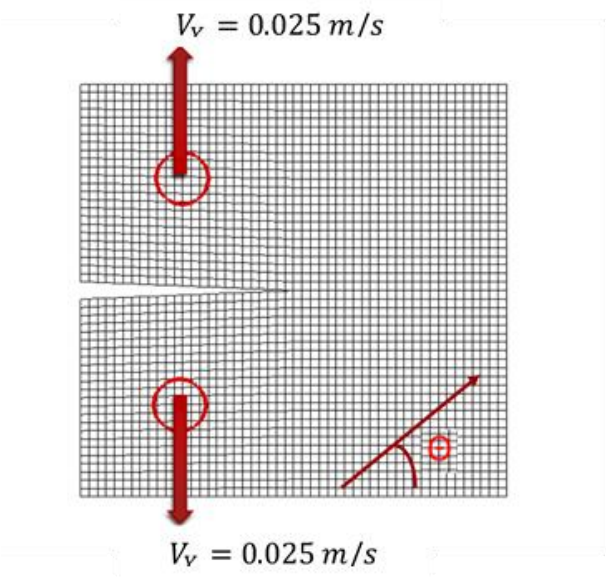

Fig. 2. Compact-tension test of a cortical bone plate.

The cortical bone is a transversely isotropic material with a fiber reinforcement. Ghajari et al. [3] verified, based on experiments, the cortical bone specimen fractures along the fiber orientation under a compact tension condition, as illustrated in Fig. 2. Therefore, this material was selected to validate the fracture pattern of a transversely isotropic lamina with different fiber orientations, Θ: $0^0, 30^0,$ and 60^0. The convergence of the

results under mesh refinement is also studied in this test. The experiment is quasi-static. To minimize dynamic effects in the numerical simulations, a small vertical velocity: $v_y = 0.025\text{m/s}$ is imposed at the nodes within the red circles in Fig. 2, which represent the loading pins, and the total applied displacement is 0.17mm as in the experiment. To compute the critical stretch for bond-breaking, we use the longitudinal and transverse energy release rates given, respectively, by $G_{If} = 2190\text{J/m}^2$ and $G_{Im} = 1030\text{J/m}^2$ [3]. The material has following material constants: E_t =22.836Gpa, $E_p = 14.8434\text{Gpa}$, $\upsilon_{tp} = 0.365$, μ_t =5.93Gpa.

The final crack patterns with different fiber orientations are shown in Fig. 3 when the loading reaches a total displacement of 0.34mm. The crack paths match the experimental results. To provide a quantitative convergence study, we plot displacement-reaction force curves in Fig. 4, for the different meshes and fiber orientations. The numerical results in this example indicate that the proposed model can predict the fracture pattern correctly with arbitrary fiber orientation.

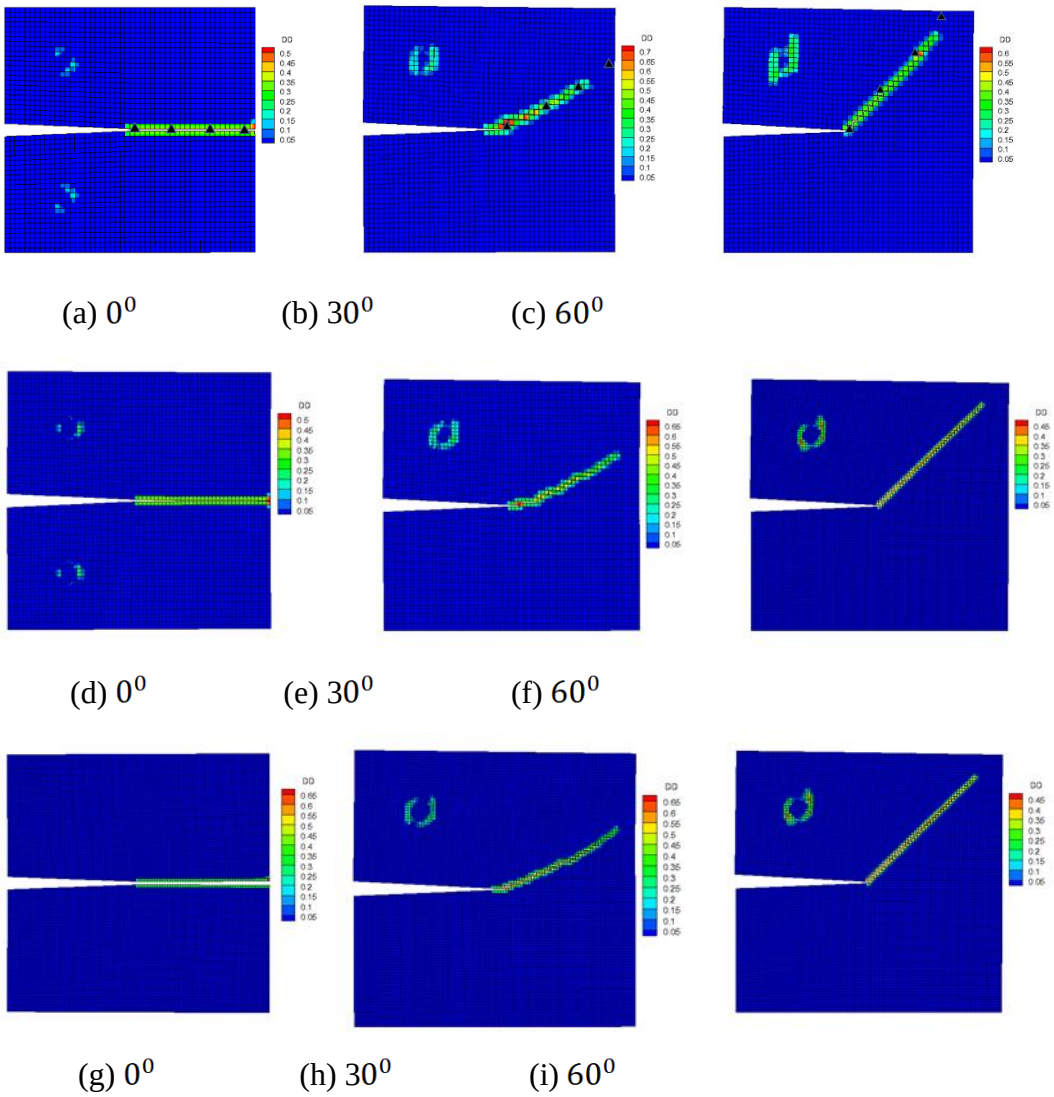

(a) 0^0 (b) 30^0 (c) 60^0

(d) 0^0 (e) 30^0 (f) 60^0

(g) 0^0 (h) 30^0 (i) 60^0

Fig. 3. Comparison of experimental ( ) and numerical crack paths for different meshes: (a)-(c) coarse mesh, (d)-(f) medium mesh, (g)-(i) fine mesh; and different fiber orientations (background: inner-layer damage).

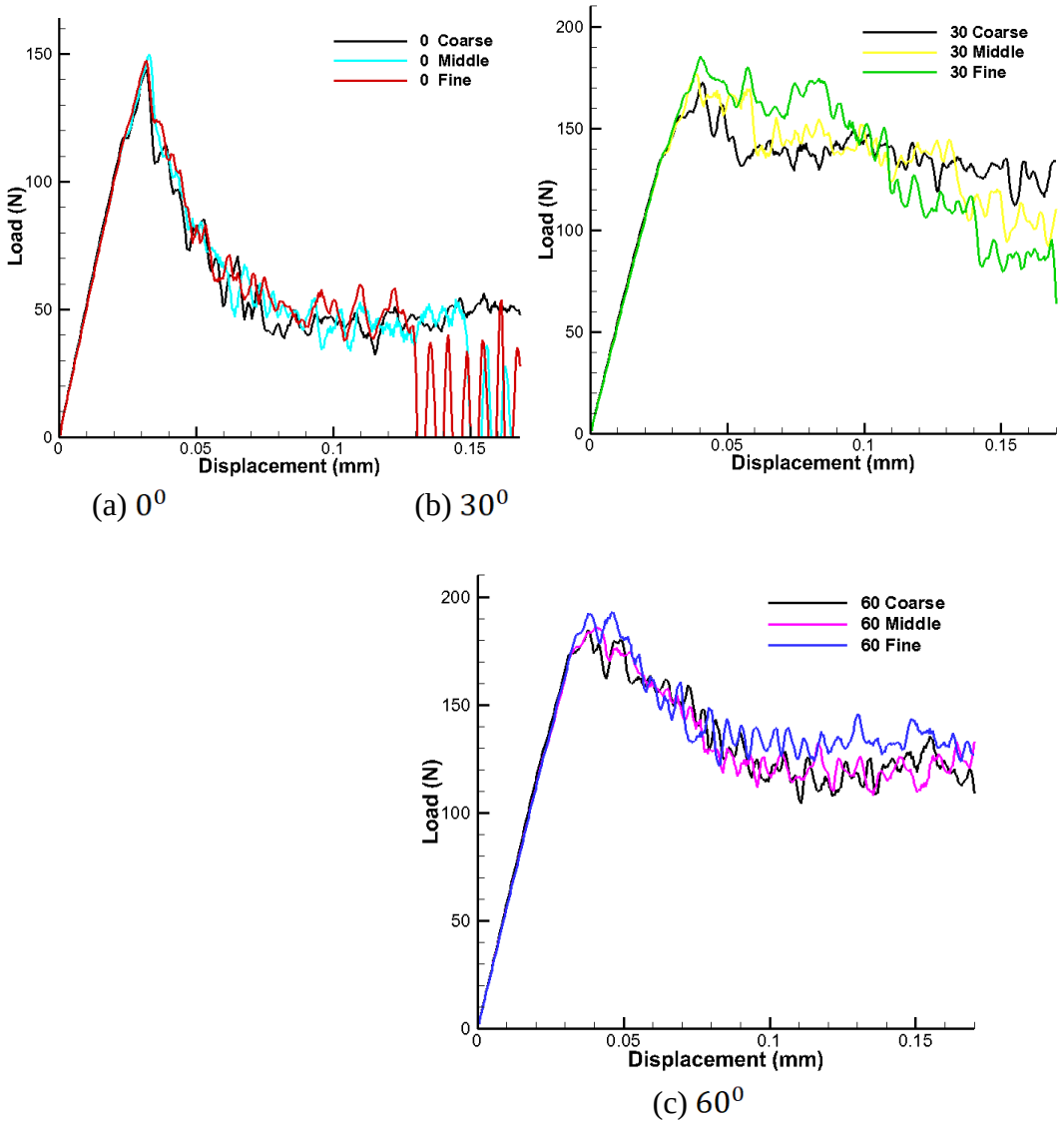

Fig. 4. Displacement-reaction force curves for different meshes and fiber orientations.

3.2 The fracture of a fiber reinforced composite laminate

Hu et al. [5] proposed an experiment to validate a numerical laminate model, as illustrated in Fig. 5. The dimensions of the specimen are: $0.2\text{m} \times 0.036\text{m} \times 0.002\text{m}$ (w × h × t) and the hole radius is: 0.003m. The specimen is made of T700 carbon/epoxy material with the material constant: E_t =142.0Gpa, $E_p = 8.73$Gpa, $\upsilon_{tp} = 0.33$, μ_t =4.49Gpa. The laminate is comprised of eight laminae with the sequence: $[45/0/-45/90]_s$. The laminate is partitioned into eight layers of quadrilateral elements as the zoomed-in view of the red square in Fig. 5. There are 33,856 elements with 33,856*4 quadrature points in this mesh. Hu et al. [5] simulated the same problem with a meshfree implementation of a peridynamic model with 229,504 nodes. Because the Gaussian integration is employed in the finite element-based implementation, a coarser mesh can be utilized to reach the same accuracy than the meshfree calculation.

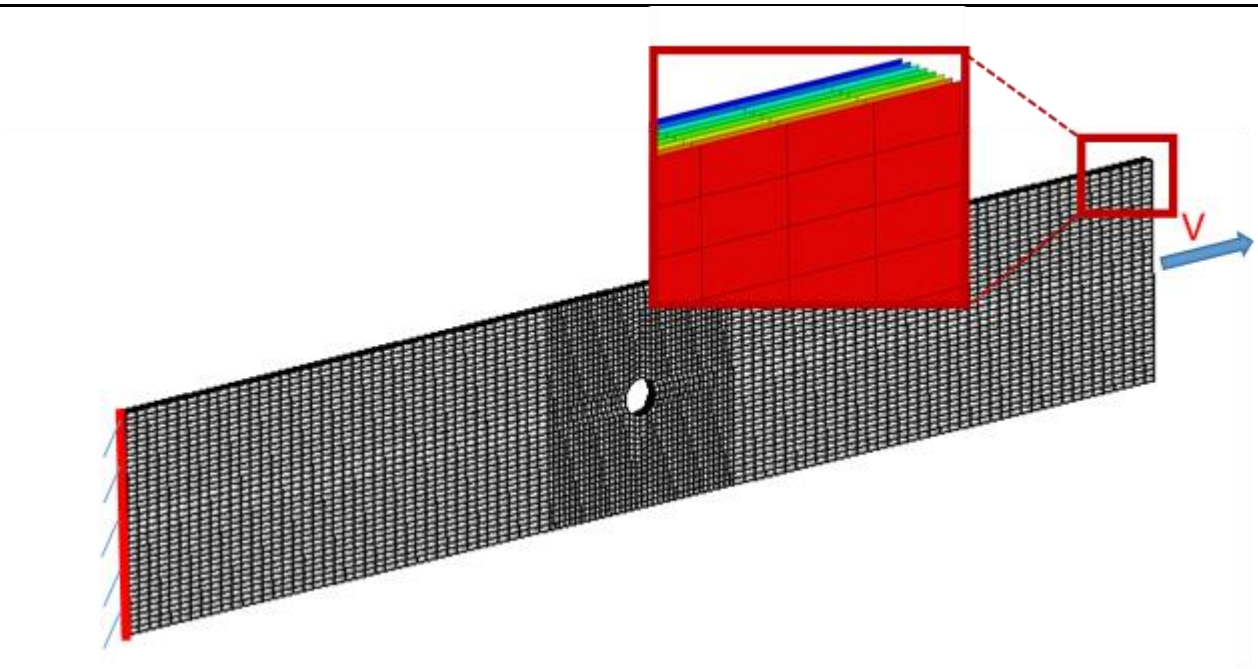

Fig. 5. Computational model for a fiber reinforced composite laminate.

The experimental displacement loading is imposed quasi-statically. Therefore, the loading velocity is set as $V = 0.025\mathrm{m/s}$ to alleviate dynamic effects. The elastic deformation of the specimen is affected by the presence of the hole. A comparison of the elastic deformation of the laminate between the numerical simulation and the experiment is shown in Fig. 6 when the displacement loading reaches 0.0003m. In Fig. 6, the longitudinal direction is also the loading direction; the vertical direction is the transverse direction to the loading direction. We observe a similar displacement field for both the longitudinal displacement (top plots) and the transverse displacement (bottom plots). To provide a quantitative comparison between the numerical and experimental results, we computed the extrema of the displacement field. From this comparison, one can find that the peridynamic results agree well with the experimental results in the longitudinal direction; the comparison is presented in Table 1. Along the transverse direction, the experiment shows a non-symmetric pattern due to a small experimental tolerance. Hence, only the deformation pattern is compared, which is shown in Figs. 6 (c) and 6 (d).

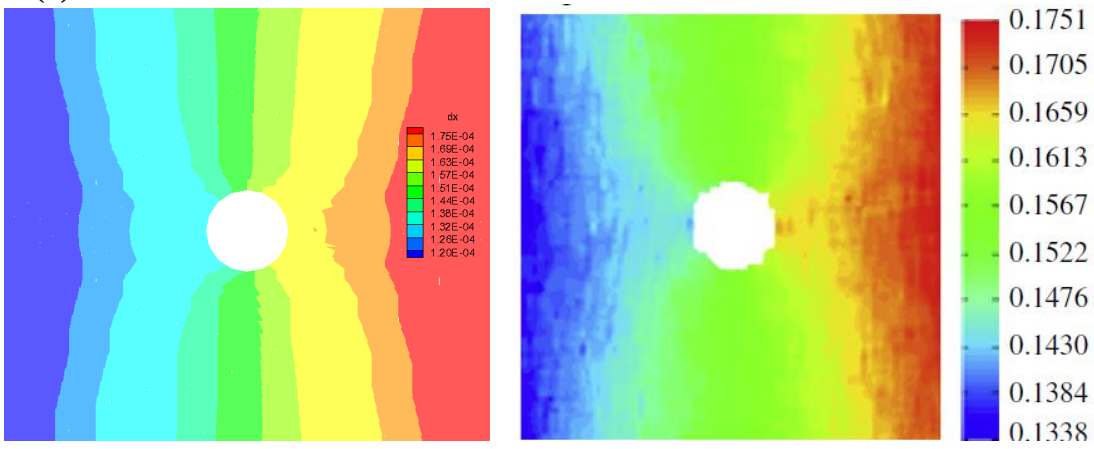

(a) Peridynamic: Longitudinal (unit: m) (b) Experiment: Longitudinal (unit: mm)

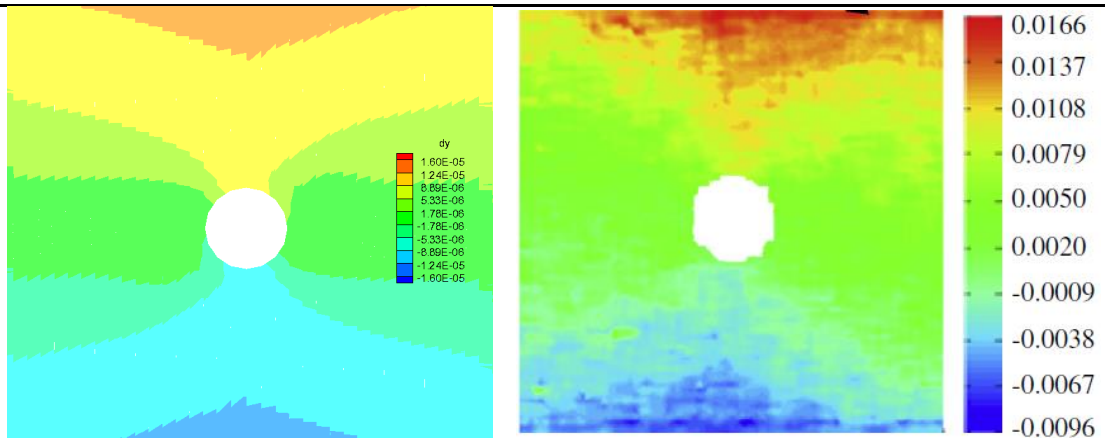

(c) Peridynamic: transverse (unit: m) (d) Experiment: transverse (unit: mm)

Fig. 6. Comparison of elastic deformation between the peridynamic simulation and the experiment.

Table 1. Characteristic values of the displacement distribution in Fig. 14.

		Peridynamic	Experiment	Error (%)
Longitudinal	Min. (mm)	0.12	0.1338	10
	Max. (mm)	0.175	0.1751	0

Inner-layer and inter-layer (delamination) damage emerge when the displacement loading is $u = 0.8mm$ as shown in Figs. 7(a) and 7(a). At this stage, the damage mainly induced by the 90^0 lamina. Subsequently, the damage zone propagates along the 90^0 and 45^0 when the displacement loading is $u = 0.805mm$ as shown in Figs. 7(b) and 8(b). The damage zone reaches the edges of the laminate when the displacement loading is $u = 0.81mm$ as shown in Figs. 7(c) and 8(c). At this stage, a strong delamination is observed. The final damage pattern of the laminate is shown in Figs. 7(d) and 8(d) when the loading is $u = 0.818mm$. Here the complex mixed damage modes are observed. The major damage direction is 90^0 with a significant delamination along 45^0 at the top ply. At the bottom ply, the -45^0 delamination can be observed because of the fiber angle. The numerical results in this test illustrates that the proposed model can capture the right elastic behavior of the laminate as well as the damage phenomena. Because of the complex mixed damage modes, it's very hard to be simulated by the other numerical methods like FEM, XFEM and meshfree methods as the best of our knowledge.

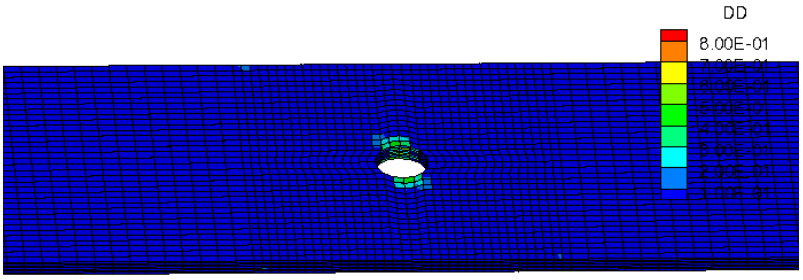

(a) $u = 0.8mm$

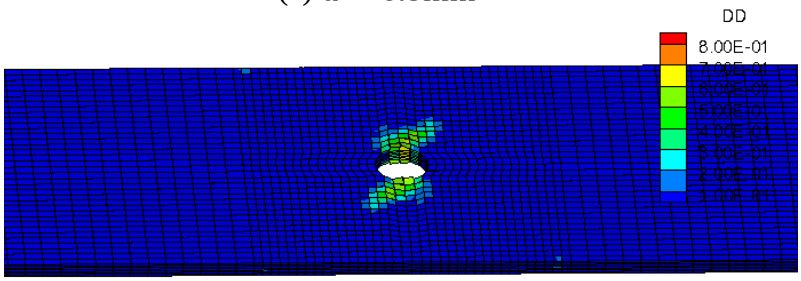

(b) $u = 0.805mm$

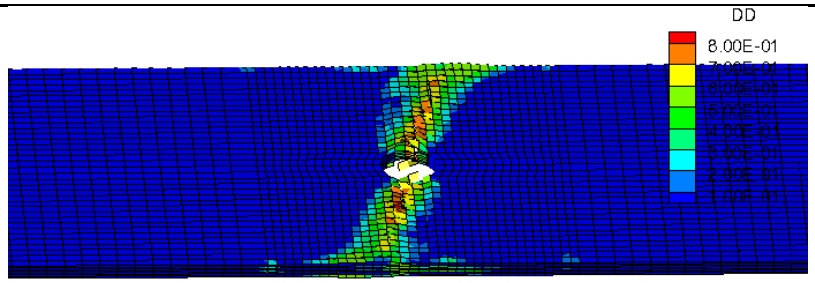

(c) u = 0.81mm

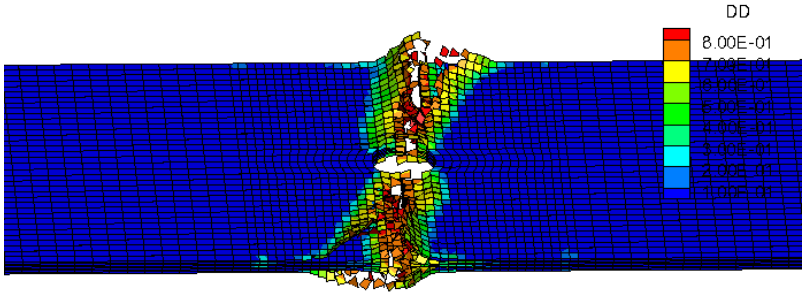

(d) u = 0.818mm

Fig. 7. Progressive inner-layer damage in a fiber reinforced composite laminate.

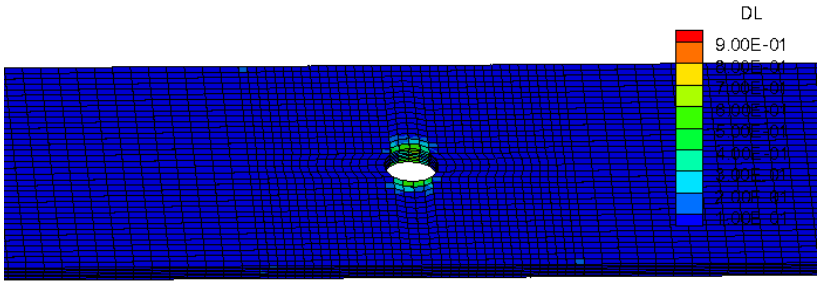

(a) u = 0.8mm

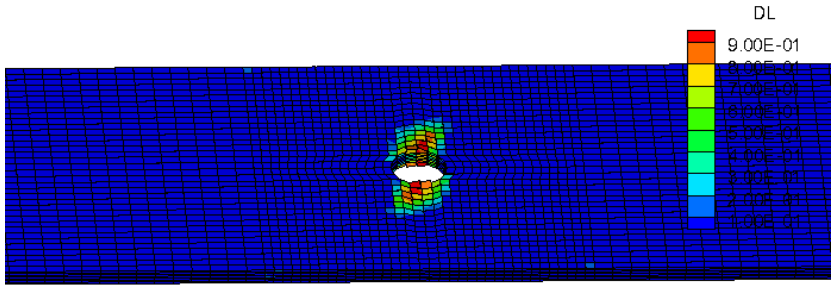

(b) u = 0.805mm

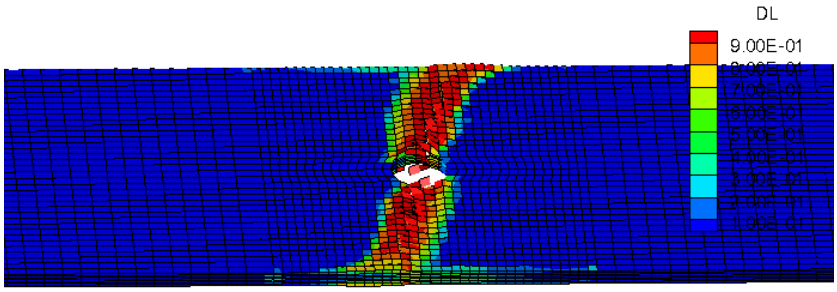

(c) u = 0.81mm

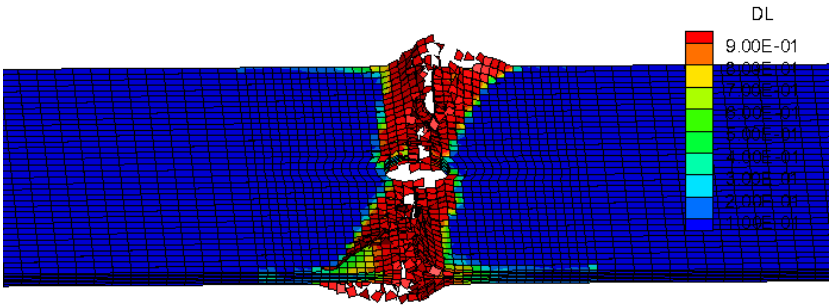

(d) u = 0.818mm

Fig. 8. Progressive delamination damage in a fiber reinforced composite laminate.

4. Conclusions

The peridynamic theory of solid mechanics has an inherent advantage in the representation of these complex damage modes. This paper presents a bond-based peridynamic model to simulate the dynamic damage process of a laminate. The numerical examples are carried out to study the convergence and performance of the proposed peridynamic model for a fiber reinforced composite laminate. The results suggest that this model can capture both the elastic response and the progressive damage phenomena of laminates with arbitrary fiber orientation under dynamic loading.

Acknowledgment

The authors would like to thank Dr. John O. Hallquist from Livermore Software Technology Corporation for his support to this research. Helpful discussions with Dr. Stewart Silling from Sandia National Laboratory, as well as with Dr. Mazdak Ghajari from Imperial College are gratefully acknowledged.

References

[1] Silling S.A., Reformulation of elasticity theory for discontinuities and long-range forces, J. Mech. Phys. Solids 48 (2000) 175–209.
[2] Wu C.T., Ren B. A stabilized non-ordinary state-based peridynamics for the nonlocal ductile material failure analysis in metal machining process, Comput. Meth. Appl. Mech. Engrg 291 (2015) 197-215.
[3] Ghajari M., Iannucci L., Curtis P., A peridynamic material model for the analysis of dynamic crack propagation in orthotropic media, Comput. Meth. Appl. Mech. Engrg. 276 (2014) 431–452.
[4] Ren B., Wu C.T., Askari E., A 3D discontinuous Galerkin finite element method with the bond-based peridynamics model for dynamic brittle failure analysis, Int. J. Impact Eng. 99 (2017) 14–25.
[5] Hu Y.L., Yu Y., Wang H., Peridynamic analytical method for progressive damage in notched composite laminates, Compos. Struct. 108 (2014) 801–810.